Li-ion Battery State of Health Estimation using LSTM with Attention Layer

Tanvir Alam Shifat
Oregon State University
Corvallis, OR, USA
shifatt@oregonstate.edu

Seyed Mahmood Shantiaeezade
Oregon State University
Corvallis, OR, USA
shantias@oregonstate.edu

Abstract

The accurate estimation of State of Health (SOH) in lithium-ion batteries is a critical challenge in prolonging their lifespan and ensuring reliability in practical applications. This study harnesses the NASA Battery Aging dataset to develop and compare two deep learning models: a traditional Long Short-Term Memory (LSTM) network and an enhanced LSTM with an added attention mechanism. Both models were trained and tested on multiple battery datasets, and their efficacy was evaluated using different performance metrics. The results indicate a marked improvement in SOH prediction accuracy with the Attention-LSTM model, demonstrating its potential to capture intricate temporal dependencies often missed by traditional LSTM networks. This research provides insights into the efficacy of attention mechanisms in time-series forecasting and proposes a promising approach for advanced battery management systems, where early and precise SOH estimation is paramount.

1. Introduction

Lithium-ion batteries are being used extensively as main power supplies in a range of applications, such as mobile phones, electric cars, autonomous underwater vehicles, and systems for storing energy [1]. Ensuring the safe operation and longevity of a battery is crucial, and this can be achieved through effective management facilitated by a battery management system (BMS). A key function of a BMS is to estimate the state of health (SOH) of the battery, offering valuable insights to safeguard against premature failure and enhance its overall durability [2]. Moreover, a battery generates electrical energy via electrochemical reactions as a power source. Over time, with repeated charging and discharging cycles, the total capacity of the battery diminishes. This decline occurs because the active substances involved in regulating output power and available capacity gradually deplete through successive chemical reactions as the battery ages, leading to a degradation in performance [3].

To date, extensive investigations have focused on estimating the SOH and predicting RUL. These endeavors can be delineated into two principal classifications: model-based methodologies, exemplified by electrochemical models and equivalent circuit models (ECMs), and data-driven approaches [3]. In an electrochemical model, the capacity of a battery is estimated by establishing a negative linear relationship between capacity and internal impedance. This estimation involves measuring the battery's internal impedance using the electrochemical impedance spectroscopy technique [4]. Within the realm of data-driven methodologies, adaptive state estimation techniques like the unscented particle filter [5], unscented Kalman filter [6], and particle filter [7] have been employed for real-time predictive tasks.

Rather than delving into the electrochemical reactions and internal failure mechanisms within batteries, model-free approaches treat the battery system as a black box, bypassing the need for explicit battery models. These methods then infer the SOH or lifespan of the battery directly from extracted features [8]. An online method for monitoring the SOH and RUL was proposed, utilizing a fusion of partial incremental capacity and feedforward neural network (FFNN) [9]. However, artificial neural networks (ANNs) typically encounter challenges such as sluggish training speed and demanding computational resources [8]. Tian et al. developed a convolutional neural network (CNN) for the estimation of electrode capacities and initial State of Charges (SOCs), referred to as electrode aging parameters (EAPs) [10]. Eddahech et al. showcased an RNN model for forecasting remaining capacity and internal resistance. This model utilizes data on state of charge (SOC) variations, pulse current, temperature, and the three most recent predictions of internal resistance values [11].

In this project, we aimed to predict the SOH of Lithium-ion batteries by implementing a long short-term memory network. Then, to improve the performance of the network, the attention mechanism was added to the network.

2. Battery SOH Estimation

2.1. NASA Battery Dataset

We utilized battery datasets sourced from the NASA Prognostics Center of Excellence Data Repository [12]. These datasets comprise eight lithium-ion batteries subjected to three distinct operational profiles: charging, discharging, and resting periods, all conducted at room temperature. The experiments involved subjecting commercially available 18650 lithium-ion cells to repeated charging and discharging cycles to accelerate aging. Charging followed the constant current constant voltage (CCCV) principle: charging at a constant current of 1.5 A until the cell voltage reached the upper limit of 4.2 V, followed by maintaining a constant voltage until the current dropped to 20 mA. Discharging occurred at a constant current of 2 A until the cell voltage reached 2.7 V, 2.5 V, 2.2 V, and 2.5 V for batteries #5, #6, #7, and #18, respectively. The experiments continued until the batteries exhibited a capacity loss of 30%, equivalent to 1.4 Ah. Additionally, the dataset included electrochemical impedance data, although it was not utilized in our study.

In actual application, batteries operate across three distinct states: charging, discharging, and resting. Precise measurement or computation of internal parameters during the discharging phase presents considerable challenges owing to the rapid temporal fluctuations in current. Recent investigations have elucidated a re-balancing phenomenon of active materials and gradient relaxation during the rest period, potentially facilitating capacity restoration. Consequently, internal battery parameters typically exhibit relative constancy or gradual variation compared to the charging or discharging phases, rendering the estimation of internal parameters challenging due to their inability to be inferred from ambiguous data. Nevertheless, batteries typically undergo a regulated charging regimen governed by predefined protocols, facilitating straightforward measurement of external electrical characteristics. Furthermore, given that discharging patterns are largely contingent upon individual usage habits and display substantial variability, the analysis of battery charging profiles is often preferred [3]. Impedance measurements are carried out during both the recharge and discharge cycles to ascertain the variation in internal parameters throughout the battery degradation process.

2.2. Definition of SOH

The battery's state of health (SOH) serves as an indicator of its overall health condition, encapsulating battery degradation characterization parameters such as capacity and internal resistance. The SOH of a battery is defined as follows,

$$SOH = \frac{C_{Real}}{C_n} \times 100\,(\%) \tag{1}$$

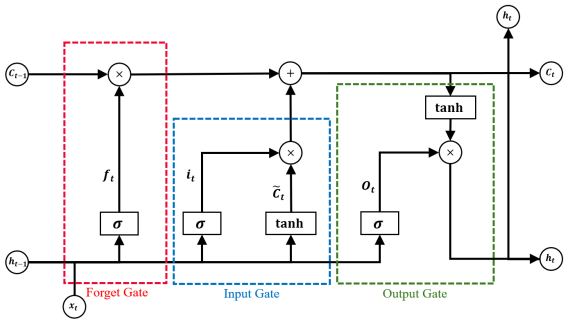

Figure 1. Architecture of LSTM cell

where C_{Real} is the battery's maximum capacity, and C_n is the nominal capacity [13].

2.3. Attention LSTM Model

Long Short-Term Memory (LSTM) stands as a widely adopted variant of Recurrent Neural Networks (RNNs). LSTM networks excel in leveraging historical data and are distinguished by their capacity to maintain long-term dependencies within such data sequences. Addressing the vanishing gradient issue inherent in traditional RNNs, LSTM networks emerge as an effective solution. Given their versatility, LSTM networks are ideally suited for tasks involving classification and the estimation of time series data, irrespective of temporal considerations [14]. The structure of LSTM is shown in Figure 1.

The gate structure, facilitated by a sigmoid layer and dot products, enables the selective transmission of information within LSTM networks. These networks incorporate three distinct gates: the forget gate, input gate, and output gate. Leveraging these gates, LSTM networks can effectively store and propagate cell states, endowing them with the capability for long-term memory retention [15].

Attention mechanisms have found application in machine translation, wherein they serve to assign probability distributions to individual words within an input sentence. Subsequently, both soft attention and hard attention models have been introduced. The soft attention model, characterized by its fully differentiable deterministic nature, diffuses across various parts of the network during attention propagation. In contrast, the hard attention model represents a stochastic process, wherein the system stochastically samples an implicit state for decoding rather than employing all implicit states simultaneously [16].

The Attention-LSTM network architecture is a powerful model for sequence learning tasks. The architecture is composed of an input layer, an LSTM layer, an attention mechanism, and an output layer.

At each time step t, the input layer receives an input vector $\mathbf{x}_t$. The LSTM layer processes the input sequence one element at a time and computes a sequence of hidden states $\mathbf{h}_t$, as per the following equations:

$$\begin{aligned}
\mathbf{f}_t &= \sigma(\mathbf{W}_f \cdot [\mathbf{h}_{t-1}, \mathbf{x}_t] + \mathbf{b}_f) \\
\mathbf{i}_t &= \sigma(\mathbf{W}_i \cdot [\mathbf{h}_{t-1}, \mathbf{x}_t] + \mathbf{b}_i) \\
\tilde{\mathbf{C}}_t &= \tanh(\mathbf{W}_C \cdot [\mathbf{h}_{t-1}, \mathbf{x}_t] + \mathbf{b}_C) \\
\mathbf{C}_t &= \mathbf{f}_t * \mathbf{C}_{t-1} + \mathbf{i}_t * \tilde{\mathbf{C}}_t \\
\mathbf{o}_t &= \sigma(\mathbf{W}_o \cdot [\mathbf{h}_{t-1}, \mathbf{x}_t] + \mathbf{b}_o) \\
\mathbf{h}_t &= \mathbf{o}_t * \tanh(\mathbf{C}_t)
\end{aligned} \tag{2}$$

Where σ denotes the sigmoid function, and $*$ denotes the Hadamard product (element-wise multiplication). The $\mathbf{W}$ terms represent weight matrices, and $\mathbf{b}$ terms represent bias vectors.

The attention mechanism then assigns a weight u_{tj} to each hidden state $\mathbf{h}_t$, which is computed by a softmax function applied to a score function, as follows:

$$u_{tj} = \frac{\exp(\text{score}(\mathbf{h}_t, \mathbf{h}_j))}{\sum_{k=1}^{n} \exp(\text{score}(\mathbf{h}_t, \mathbf{h}_k))} \tag{3}$$

The score function usually takes the form of a dot product, but can also be a more complex function, such as a feed-forward neural network with learned weights. The weighted sum of the hidden states is then used as the context vector $\mathbf{v}$:

$$\mathbf{v} = \sum_{j=1}^{n} u_{tj} \mathbf{h}_j \tag{4}$$

Finally, the context vector $\mathbf{v}$ is used by the output layer to generate the output $\mathbf{y}$, which completes the forward pass of the LSTM-attention network.

3. Result Analysis

3.1. Data Analysis

As explained in the previous section, the NASA Battery Dataset comprises data from experiments conducted on four lithium-ion batteries (identified as B05, B06, B07, B18, B33, B34, B46, B47 and B48) subjected to various operational profiles to study their performance and aging process. These operational profiles include charging, discharging, and impedance measurements at room temperature. A list of dataset sizes for different batteries is presented in Table I.

Figure 2 shows the behaviour of the charging and discharging cycle for B05. During the charging phase, we observe a distinct voltage, current, and temperature behaviour. Initially, the voltage rapidly climbs to a plateau, suggesting a constant-current charging phase where the battery is

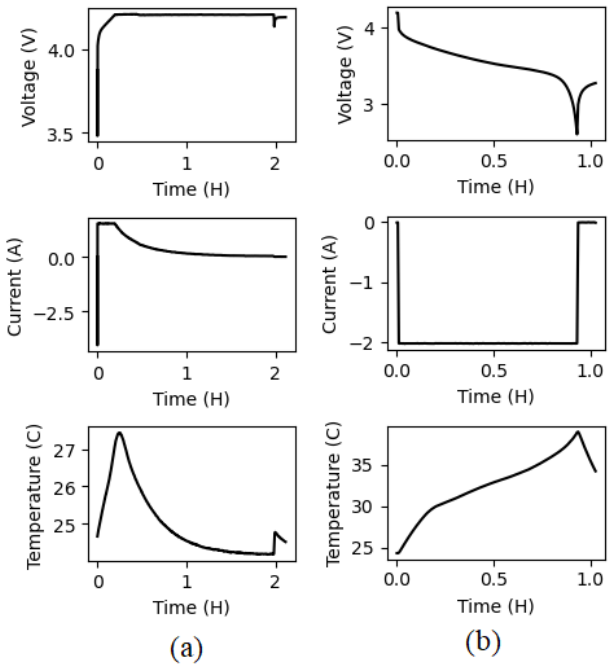

Figure 2. (a) Charging of B05, (b) Discharging of B05)

charged at a high current until it reaches a certain voltage threshold. Following this, the voltage levels off, indicating a transition to a constant-voltage phase where the current gradually tapers down to maintain the voltage level, minimizing stress on the battery as it approaches full charge. Concurrently, the temperature profile shows a sharp rise at the beginning, reflecting the exothermic nature of the charging process.

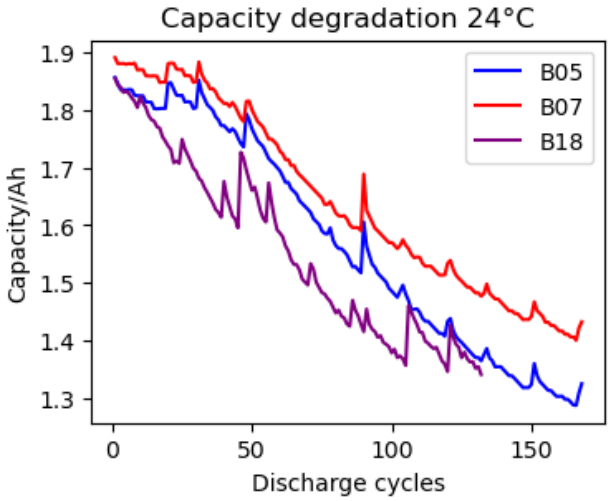

Figure 3. (a) Charging of B05, (b) Discharging of B05

Dataset	Size	Discharge Cycles
B05	50285×9	168
B07	50285×9	168
B18	34866×9	129
B33	42200×9	195
B34	45909×9	195
B46	23478×9	72
B47	23478×9	72
B48	23478×9	72

Table 1. NASA Battery Dataset Size.

During the discharge cycle, the voltage starts at its highest and drops gradually as the battery delivers energy, with a noticeable steep decline as it nears complete discharge. This voltage sag is characteristic of the depletion of available energy in the battery's physics. Temperature trends upwards throughout the discharging phase, which is typical due to the battery's internal resistance and the energy being expended as work and heat.

Figure 3 illustrates the capacity degradation of B05, B07, and B18 batteries over their respective discharge cycles at 24 degrees Celsius. All three battery lines show a downward trend, indicating a loss of capacity with each discharge cycle—a common phenomenon in batteries known as cycling degradation. Battery B05 starts off with the highest capacity but experiences a rapid decline that slows down after approximately 50 cycles. Battery B07 has a somewhat lower initial capacity and shows a steadier but consistent degradation over time. Lastly, Battery B18, while starting off around the same capacity as B07, demonstrates the most gradual decline in capacity over the 150 cycles depicted.

Hyperparameter	LSTM	Attention-LSTM
Optimizer	Adam	Adam
No. of hidden layers	3	3
Learning rate	0.001	0.005
Batch Size	64	32
Epoch	50	50
Loss function	MAE	MAE

Table 2. Model hyperparameters.

3.2. Model Build-up

The described model is a sequential neural network implemented using TensorFlow and Keras on Python. The architecture of the model begin with an LSTM layer with 32 units is the first layer of the model. This layer is designed to process data sequences. The `input_shape` parameter is dynamically set based on the shape of the training dataset, specifically, `trainX.shape[1]` for the sequence length and `trainX.shape[2]` for the number of features per timestep. A layer with a rate of 0.2 prevents overfitting by randomly setting a fraction of input units to 0 at each update during training time. A **Dense** layer with 50 units and ReLU (Rectified Linear Unit) activation function. This fully connected layer serves as an additional hidden layer to increase the model's capacity. The final layer of the model is a **Dense** layer with a single unit. This output layer is designed to produce a single continuous output, making it suitable for regression tasks. A list of hyperparameters is shown in Table 2.

Using the hyperparameters reported in Table 2, the training and validation losses are shown in Figure 4 and 5 for LSTM and Attention-LSTM respectively.

To evaluate the model's performance, several metrics

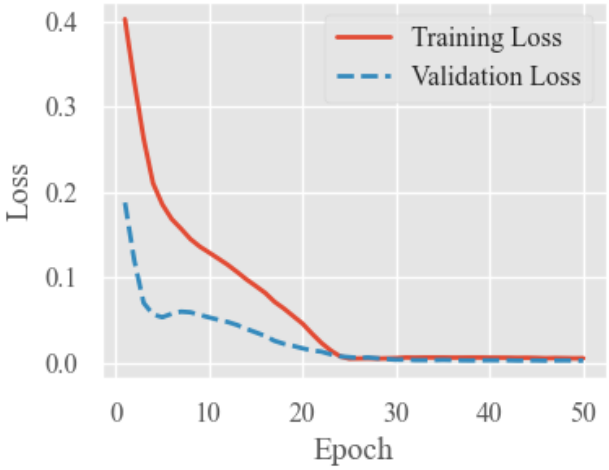

Figure 4. LSTM learning curves.

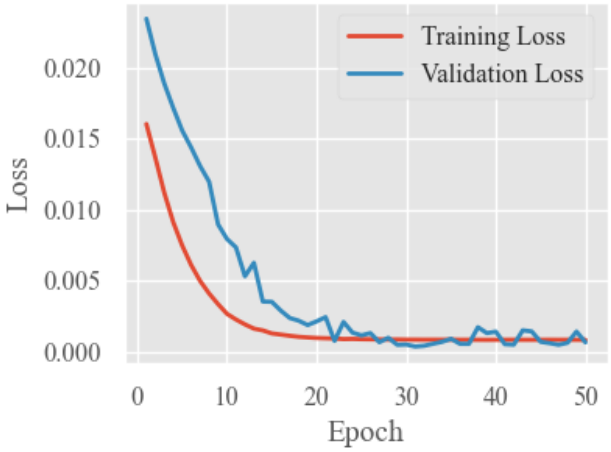

Figure 5. Attention-LSTM learning curves.

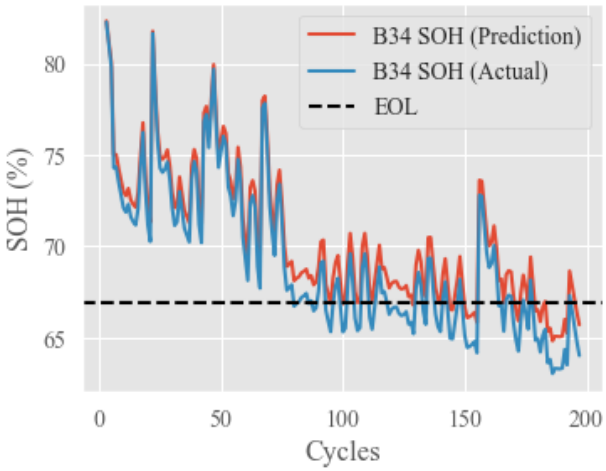

Figure 6. LSTM Prediction on B34.

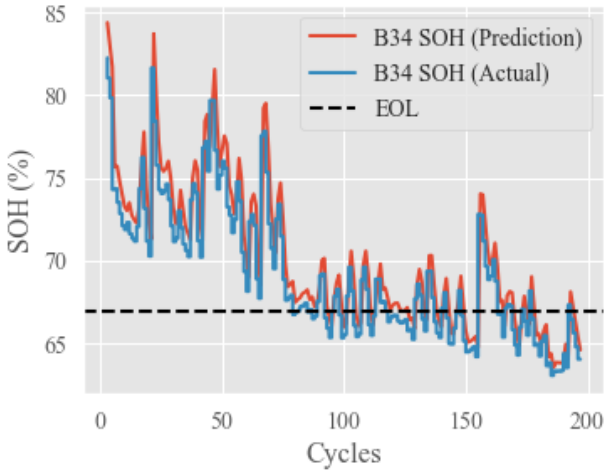

Figure 7. Attention-LSTM Prediction on B34.

have been obtained from the predicted SOH. Thef first one is Mean Absolute Error (MAE), which is defined as:

$$\text{MAE} = \frac{1}{n}\sum_{i=1}^{n}|real\_SOH_i - predicted\_SOH_i| \quad (5)$$

where, n is the number of samples, $real\_SOH_i$ is the actual value of the State of Health (SOH) for the i^{th} sample, $predicted\_SOH_i$ is the predicted value of the SOH for the i^{th} sample.

The Root Mean Squared Error (RMSE) is defined as:

$$\text{RMSE} = \sqrt{\frac{1}{n}\sum_{i=1}^{n}(real\_SOH_i - predicted\_SOH_i)^2} \quad (6)$$

The Coefficient of Determination, or R2 Score, is defined as:

$$R^2 = 1 - \frac{\sum_{i=1}^{n}(real\_SOH_i - predicted\_SOH_i)^2}{\sum_{i=1}^{n}(real\_SOH_i - \bar{real\_SOH})^2} \quad (7)$$

where $\bar{real\_SOH}$ is the mean of actual SOH values.

Together, these metrics give a comprehensive view of the model's prediction accuracy, with MAE and RMSE focusing on the average error magnitude and R2 score, indicating how well the predictive model can explain the variation in the data.

3.3. SOH Estimation

For the LSTM model, the SOH estimation using a single Battery input results in very poor performance, so we have trained the LSTM model using B05, B07, B18, and B33. Both the LSTM and Attention-LSTM models are then tested on the B34 dataset.

Figures 6 and 7 illustrate the performance of the LSTM and Attention-LSTM in predicting the SOH of Battery B34. The solid blue line represents the actual measured SOH of the battery across the cycles, while the solid red line represents the SOH predicted by the model. Figure 6 shows the LSTM model's predictions. The LSTM model's ability to track the SOH trend is quite good, although some discrepancies between prediction and actual measurements can be seen, particularly at the peaks and troughs. In the case of Attention-LSTM, we can observe that the prediction line closely follows the actual SOH line, albeit with some deviations. This indicates that the Attention-LSTM model has learned to approximate the battery's degradation behaviour over time with reasonable accuracy. However, there are instances where the prediction deviates significantly from the actual measurements, reflecting the challenges in modelling the complex behaviour of battery health deterioration.

The dashed horizontal line labelled 'EOL' signifies the End of Life threshold for the battery, which is the point at which the battery is considered to have insufficient capacity to meet operational requirements—often set at 80% SOH.

Finally, the trained model was tested on all the battery datasets. Since the LSTM model was trained on B05, B07, B18, and B33, it shows pretty good result on these datasets. Therefore, the legit comparison between LSTM and Attention-LSTM can be seen from B34 where all the datasets are unknown to the model. It can be seen that Attention-LSTM outperforms LSTM in all three performance metrics as shown in Table 3.

4. Future Work and Improvements

Although this work shows quite good results in Battery SOH estimation, there are some scopes for improvement.

Battery	LSTM			Attention LSTM		
	RMSE	MAE	R2	RMSE	MAE	R2
B05	0.0078	0.0069	0.9926	0.019	0.018	0.9512
B07	0.0066	0.0055	0.9926	0.023	0.021	0.9132
B18	0.0066	0.0059	0.9929	0.02	0.019	0.9355
B33	0.0061	0.0050	0.9880	0.015	0.014	0.9347
B34	0.0088	0.0079	0.9565	0.01	0.01	0.9495
B46	0.0149	0.0135	0.9338	0.007	0.006	0.9865
B47	0.0162	0.0150	0.9201	0.006	0.005	0.9918
B48	0.0135	0.0126	0.9148	0.007	0.006	0.9737

Table 3. Comparative performance metrics of LSTM and Attention-LSTM models across battery datasets.

A primary area of exploration is the integration of multi-dimensional data, such as temperature and charge/discharge rates, to provide the models with a more comprehensive feature set for SOH prediction.

In terms of model architecture, experimenting with deeper networks and different forms of attention mechanisms could further improve prediction accuracy. There is also potential in exploring hybrid models that combine the strengths of LSTM with other machine learning techniques, such as convolutional neural networks (CNNs) for feature extraction from time-series data.

From an application standpoint, real-time SOH estimation in battery management systems is a promising direction. Implementing these models online would allow for continuous monitoring and immediate decision-making, crucial for safety-critical applications like electric vehicles and aerospace.

Lastly, expanding the dataset to include a broader range of battery types and aging processes could significantly enhance the generalizability of the models. Long-term studies that capture the entire lifespan of batteries under various cycles and loads will provide a richer dataset, paving the way for models that can more confidently predict battery life.

5. Conclusion

This study presents a comprehensive performance analysis of two deep-learning models for Li-ion battery SOH prediction. The LSTM model reliably captured the temporal degradation patterns within the NASA Battery Aging dataset. However, introducing an attention mechanism enhanced the LSTM's ability to focus on critical sequences within the data, thereby refining the accuracy of the SOH predictions. The Attention-LSTM model demonstrated superior performance across all considered metrics—RMSE, MAE, and R^2—signifying its robustness and potential applicability in real-world battery health monitoring scenarios. The research underscores the value of integrating attention mechanisms with recurrent neural networks, presenting a substantial step forward in battery health management. Future work will explore integrating these models into battery management systems for various applications, including electric vehicles and grid storage, to enhance the operational efficiency and safety of these critical energy storage technologies.

References

[1] J. Lee and I. Lee, "Online estimation algorithm of soc and soh using neural network for lithium battery," in *2021 IEEE 3rd Eurasia Conference on IOT, Communication and Engineering (ECICE)*, IEEE, 2021, pp. 568–571.

[2] M. A. Kamali, A. C. Caliwag, and W. Lim, "Novel soh estimation of lithium-ion batteries for real-time embedded applications," *IEEE Embedded Systems Letters*, vol. 13, no. 4, pp. 206–209, 2021.

[3] Y. Choi, S. Ryu, K. Park, and H. Kim, "Machine learning-based lithium-ion battery capacity estimation exploiting multi-channel charging profiles," *IEEE Access*, vol. 7, pp. 75 143–75 152, 2019.

[4] K. Goebel, B. Saha, A. Saxena, J. R. Celaya, and J. P. Christophersen, "Prognostics in battery health management," *IEEE instrumentation & measurement magazine*, vol. 11, no. 4, pp. 33–40, 2008.

[5] D. Liu, X. Yin, Y. Song, W. Liu, and Y. Peng, "An online state of health estimation of lithium-ion battery using unscented particle filter," *IEEE Access*, vol. 6, pp. 40 990–41 001, 2018.

[6] G. L. Plett, "Extended kalman filtering for battery management systems of lipb-based hev battery packs: Part 3. state and parameter estimation," *Journal of Power sources*, vol. 134, no. 2, pp. 277–292, 2004.

[7] A. Guha and A. Patra, "State of health estimation of lithium-ion batteries using capacity fade and internal resistance growth models," *IEEE Transactions on Transportation Electrification*, vol. 4, no. 1, pp. 135–146, 2017.

[8] T. Oji, Y. Zhou, S. Ci, F. Kang, X. Chen, and X. Liu, "Data-driven methods for battery soh estimation: Survey and a critical analysis," *IEEE Access*, vol. 9, pp. 126 903–126 916, 2021.

[9] S. Zhang, B. Zhai, X. Guo, K. Wang, N. Peng, and X. Zhang, "Synchronous estimation of state of health and remaining useful lifetime for lithium-ion battery using the incremental capacity and artificial neural networks," *Journal of Energy Storage*, vol. 26, p. 100 951, 2019.

[10] J. Tian, R. Xiong, W. Shen, and F. Sun, "Electrode ageing estimation and open circuit voltage reconstruction for lithium ion batteries," *Energy Storage Materials*, vol. 37, pp. 283–295, 2021.

[11] A. Eddahech, O. Briat, N. Bertrand, J.-Y. Delétage, and J.-M. Vinassa, "Behavior and state-of-health monitoring of li-ion batteries using impedance spectroscopy and recurrent neural networks," *International Journal of Electrical Power & Energy Systems*, vol. 42, no. 1, pp. 487–494, 2012.

[12] NASA, *Li-ion battery aging datasets*, 2008. [Online]. Available: `https://catalog.data.gov/dataset/li-ion-battery-aging-datasets`.

[13] S. Bamati and H. Chaoui, "Lithium-ion batteries long horizon health prognostic using machine learning," *IEEE Transactions on Energy Conversion*, vol. 37, no. 2, pp. 1176–1186, 2022.

[14] U. Yayan, A. T. Arslan, and H. Yucel, "A novel method for soh prediction of batteries based on stacked lstm with quick charge data," *Applied Artificial Intelligence*, vol. 35, no. 6, pp. 421–439, 2021.

[15] Y. Zhang, R. Xiong, H. He, and M. G. Pecht, "Long short-term memory recurrent neural network for remaining useful life prediction of lithium-ion batteries," *IEEE Transactions on Vehicular Technology*, vol. 67, no. 7, pp. 5695–5705, 2018.

[16] Z. Lin, L. Cheng, and G. Huang, "Electricity consumption prediction based on lstm with attention mechanism," *IEEJ Transactions on Electrical and Electronic Engineering*, vol. 15, no. 4, pp. 556–562, 2020.